

## Feature Article

## A new approach to the investigation of nanoparticles: Electron tomography with compressed sensing

John Meurig Thomas<sup>a,\*</sup>, Rowan Leary<sup>a,\*</sup>, Paul A. Midgley<sup>a</sup>, Daniel J. Holland<sup>b</sup><sup>a</sup> Department of Materials Science and Metallurgy, University of Cambridge, Pembroke Street, Cambridge CB2 3QZ, UK<sup>b</sup> Department of Chemical Engineering and Biotechnology, University of Cambridge, New Museums Site, Pembroke Street, Cambridge CB2 3RA, UK

## ARTICLE INFO

## Article history:

Available online 22 October 2012

Based on the oral presentation (by JMT) at the 244th ACS National Meeting, Philadelphia, August 2012, in the Division of Colloid and Surface Chemistry Symposium honouring Egon Matijević on the occasion of his 90th birthday

## Keywords:

Electron tomography  
Compressed sensing  
Nanoparticles  
3D image reconstruction  
Sparsity

## ABSTRACT

The principal purpose of this contribution is to illustrate the potential of compressed sensing electron tomography for the characterisation of nanoparticulate materials that are vulnerable to electron beam damage. Not only is there growing interest in nanoparticles of organic materials in medical and allied contexts, there is also the need to investigate nanoparticles and nanoclusters of metals supported on biological macromolecular entities in the context of drug delivery. A qualitative account of the principles of electron tomography is outlined with illustrations from the field of heterogeneous catalysis, where electron beam damage is less of an issue, and an appendix deals with more quantitative aspects of how compressed sensing promises to expand the range of samples that have hitherto been accessible to investigation.

© 2012 Elsevier Inc. All rights reserved.

## 1. Introduction

The technique of tomography is currently applied widely for the study of macro-objects in medicine and in engineering using X-rays or positrons as the probing radiation. In essence, tomography entails reconstructing the three-dimensional (3D) structure of an object from a series of two-dimensional (2D) projection images. Electron tomography (ET) is a relatively new tool for probing nanoparticulate and other nano-structured materials, but its use has grown rapidly in recent years, as may be gauged from Fig. 1.

Two of us (PAM and JMT) have hitherto exploited ET, which is capable of resolutions of ca. 10 Å, largely for the investigation of the morphologies, spatially-discriminating chemical compositions and defect properties of nanoclusters and nanoparticles of bimetallic heterogeneous catalysts [1–4]; but our group has also identified and demonstrated the power of the technique when allied to the so-called approach of compressed sensing (CS) – which we discuss below – for other kinds of investigation [5,6].

It is our conviction that ET allied to CS could contribute significantly to the now burgeoning field of nanoparticles in medicine and pharmacy, in which fine particles of entirely organic or biological materials – which are notoriously vulnerable to electron beam

damage – are finding increasing use [7,8]. A very recent example entails the use of aggregates of poly(lactic-co-glycolic acid) nanoparticles to which are attached tissue plasminogen activator (tPA) for the treatment of atherosclerosis and the avoidance of blood clot formation during a stroke [8].

## 2. Methods

ET may be recorded either by the use of conventional transmission electron microscopy (TEM) under so-called bright-field (BF) illumination [9], or using high-angle annular dark-field scanning transmission electron microscopy (HAADF-STEM), the technique we favour. A diagrammatic summary is shown in Fig. 2. It has been shown elsewhere [10] that there are distinct advantages in using the HAADF mode in preference to the BF method. Moreover because the signal recorded under HAADF conditions directly reflects the atomic number ( $Z$ ) contrast of the specimen, there are additional analytical advantages to be gained by utilising this mode. Indeed, Fig. 3 illustrates this point.

Qualitatively we may illustrate the essence of tomographic reconstruction with the diagrams shown in Fig. 2, where *inter alia*, the notion of back-projection is given, yielding a 3D reconstruction or ‘tomogram.’ Because of the practical limitations imposed by the relative disposition and size of the sample holder with respect to the pole-piece of the microscope, a so-called ‘missing wedge’ of

\* Corresponding authors. Fax: +44 (0)1223334567 (J.M. Thomas).

E-mail addresses: jmt2@cam.ac.uk (J.M. Thomas), rkl26@cam.ac.uk (R. Leary).

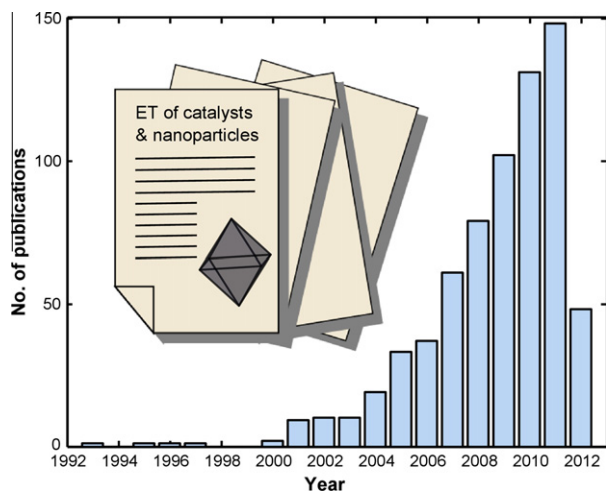


**Fig. 1.** The growing application of ET to the study of catalysts and nanoparticles, as tracked by the annual number of publications. Source: ISI Web of Knowledge, 02/08/12. Search term: “(electron tomography AND (catalyst\* OR nanoparticle\*))”.

information is un-sampled by the tilt-series images and inevitably affects the reconstruction process. Elsewhere we have shown how quantitative ET may be carried out in the investigation of bimetallic nanocluster catalysts distributed over the inner surface of mesoporous silica [11]. A summary of the kind of information that may be retrieved is shown in Fig. 4.

We outline below (and explain in greater detail in the appendix) how, with CS, it is possible to retrieve valuable information pertaining to specimens that are vulnerable, to a greater or lesser extent, to electron beam damage, as well as specimens that, for other reasons, are not amenable to investigation by conventional ET. The actual examples of the use of CS-ET that we cite here are, in fact, ones that are relatively stable in the electron beam, but they serve as instructive proof-of-principle studies.

CS has arisen from information theorists and mathematicians concerned with signal retrieval. CS techniques are particularly use-

ful in applications in which one cannot, for one reason or another, record a large number of measurements of the signal that is to be reconstructed. It has proven useful in magnetic resonance imaging (MRI) [12,13], for instance, and several accounts have been given detailing the essence of the ‘compressive’ measurement and recovery procedures [12,14–17].

The aim of CS is to recover a signal from fewer measurements than would normally be considered necessary, be it an angiogram in MRI, a spectrum in nuclear magnetic resonance, an image in astronomy, or a tomogram in ET. In order to reconstruct the signal from a small number of measurements, it is necessary to introduce some prior knowledge into the problem. In the case of CS, this prior knowledge is that the signal of interest is ‘information limited’ or ‘sparse.’ Here, ‘information’ refers to the number and location of non-zero elements in the signal. A signal is said to be ‘sparse’ if the number of non-zero elements is significantly less than the total number of elements comprising the signal. In the context of ET, these non-zero elements would most readily correspond to voxels (volume pixels) in the tomogram.

However, what makes CS so powerful is that it is not necessary for the signal itself to be sparse; instead the signal can be transformed into some other domain in which it is sparse. CS uses the idea that signals can be represented sparsely to recover images from incompletely sampled data by finding the sparsest solution that is consistent with the measured data.

In order to apply CS it is essential that the measurements are ‘incoherent’ with respect to the basis in which the signal is sparsely represented. This entails two aspects: (1) each data point measured must contain information about many of the elements that comprise the final signal, and (2) any artefacts arising from incomplete measurements should appear noise-like (i.e. not be sparse) in the domain in which the signal is represented sparsely. The first of these two points is readily addressed by ET data sets, as each measurement will comprise a projection through the sample and therefore contain information about every part of the sample through which the electron beam has passed. The second point is more difficult to conceptualise, but essentially means that artefacts that arise from incomplete sampling from any one part of a signal should be spread throughout as much of the remainder of the

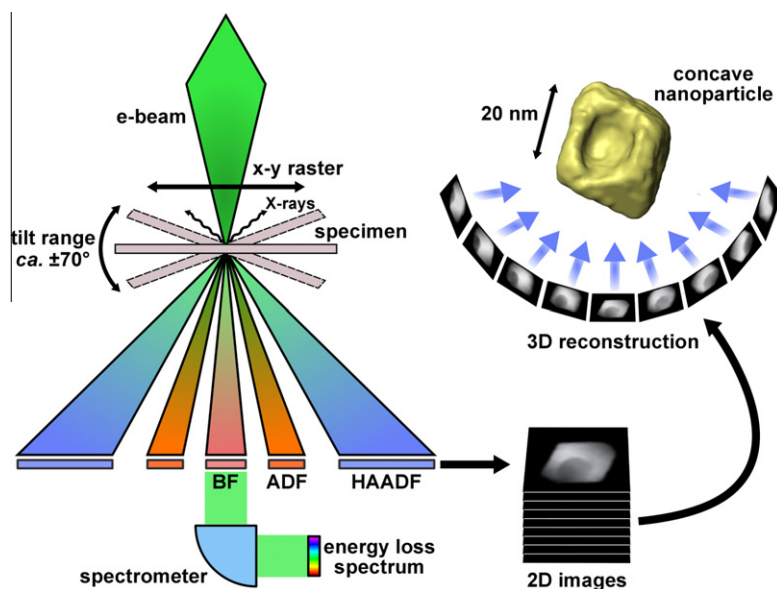


**Fig. 2.** The essence of ET: an angular series of 2D projection images is recorded by tilting the specimen in the (scanning) transmission electron microscope. The ‘tilt-series’ of images are then back-projected into space to obtain a 3D reconstruction. A variety of signals may be recorded, including bright-field (BF), annular dark-field (ADF) and high-angle annular dark-field (HAADF) signals. The BF detector can be removed to allow the transmitted electrons to pass through to a spectrometer and form an energy-loss spectrum.

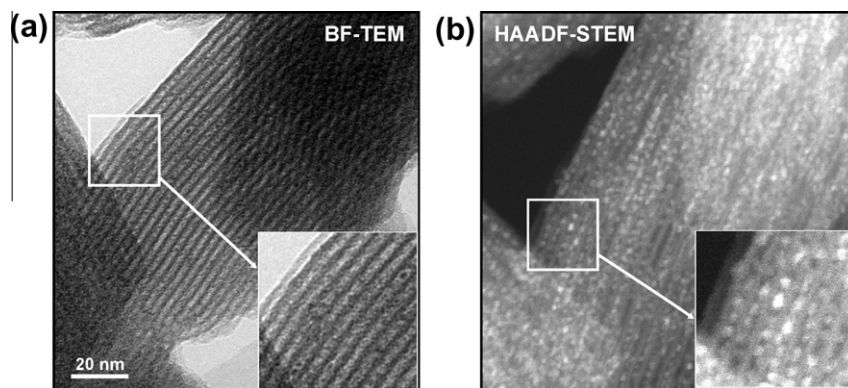


**Fig. 3.** An illustrative example of the efficacy of HAADF-STEM for the study of supported metallic nanoparticles. The (Pt,Ru) nanoparticles supported on mesoporous silica, almost invisible in BF-TEM (a), are clearly seen in the HAADF image (b) [10].

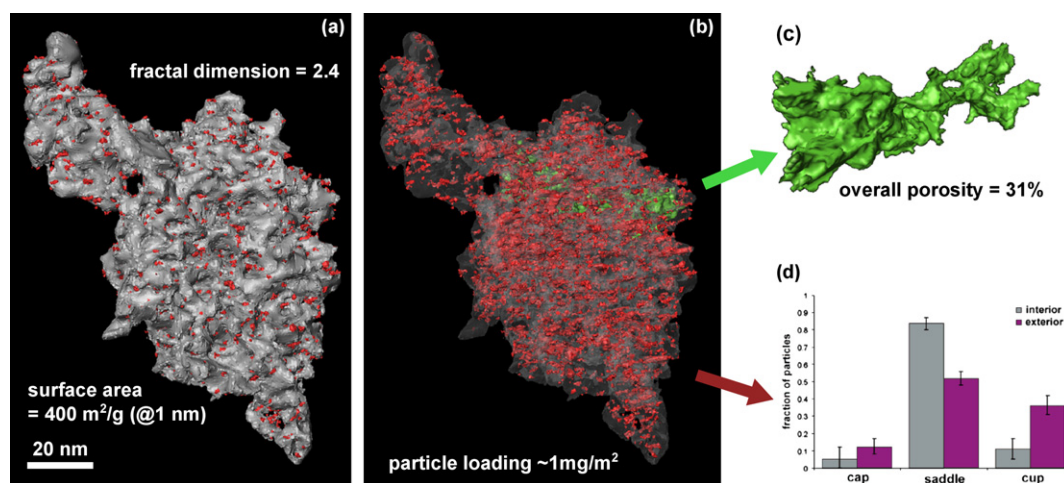


**Fig. 4.** (a) Surface rendering of an ET reconstruction of (Pt,Ru) nanocatalysts (red) supported on a disordered mesoporous silica (grey). (b) The reconstruction shown with the support made partially transparent to reveal the internal distribution of the nanocatalysts. (c) A small part of the pore structure shown as a solid object. From the reconstruction, the catalyst loading, overall porosity and surface area were determined. The surface dimension of the pore structure was found to be fractal in nature. (d) By classifying the surface curvature of the support, the nanocatalysts were found to prefer to be anchored at saddle-points on the support surface [11].

image as possible. This means that the location of the true signal will appear with a high intensity relative to any artefacts and therefore can be recovered accurately during the reconstruction.

We illustrate the concepts underlying CS using an image of a simple object shown in Fig. 5a. This image can be represented sparsely by transforming it into the gradient domain, via a spatial finite differences transform. The gradient domain representation is shown in Fig. 5b, where there are few non-zero pixels; only those

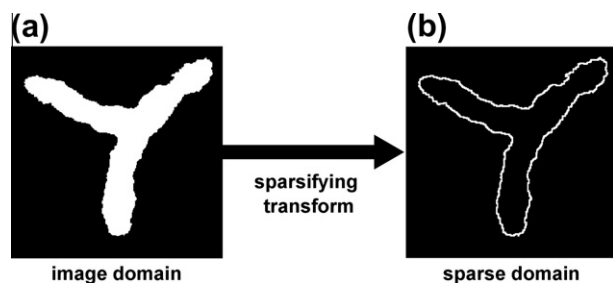


**Fig. 5.** The concept of sparse representation: a sparse representation (b) of the image (a) is obtained by the application of an appropriate sparsifying transform. In this example, the information in the simple cartoon-like image (a) can be captured by a small number of non-zero pixels in the gradient domain (b). The sparsifying transform, is a spatial finite differences operator.

capturing the important information from the image in Fig. 5a – the boundary of the object – being non-zero. The gradient domain is suitable for sparse representation of cartoon-like images, such as Fig. 5a, consisting of homogeneous regions with sharp boundaries, and the overall gradient sparsity is often expressed via the so-called ‘total variation’ (TV).

For more complex images, a wide variety of transforms exist, such as the so-called discrete cosine and discrete wavelet transforms, which form the basis of JPEG image compression algorithms, familiar from digital photography. The effectiveness of image compression algorithms lies in the fact that it is often only necessary to retain the largest coefficients in the sparse domain, a small fraction of the total, yet still recover the original image with minimal loss of information when applying the inverse transform.

Given that it is possible to represent an image (or other signal of interest) sparsely, capturing the information content of the image in a reduced amount of data, it then follows that it should be possible to measure fewer data points than pixels in the image during the initial acquisition. In other words, it should be possible to acquire the image directly in compressed form. CS provides a mathematical foundation that proves when and how this is possible. By applying these principles to reduce the number of projections that need to be acquired in ET, it is clear that CS has the potential to make a significant impact.

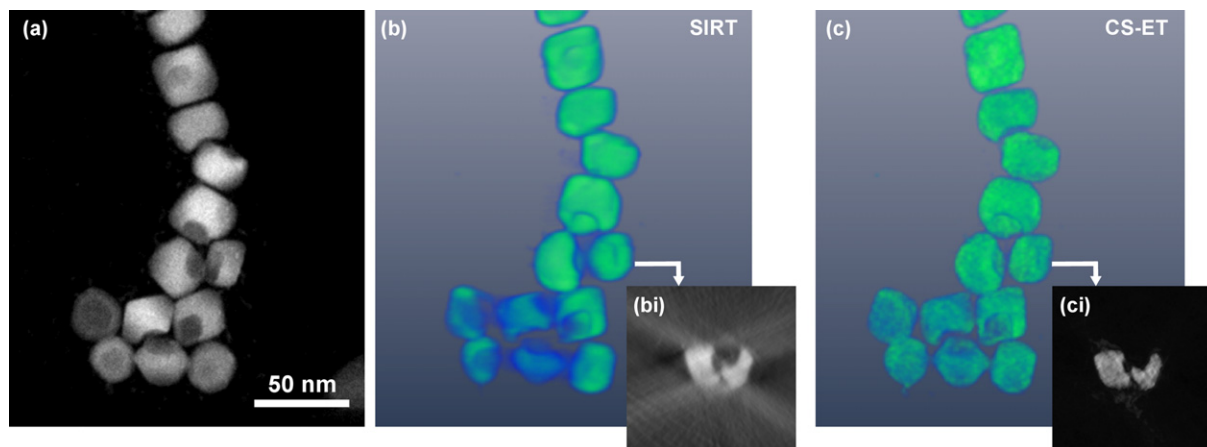


**Fig. 6.** HAADF-STEM image of concave iron oxide nanoparticles from an ET tilt-series. (b) and (c) 3D voxel projection visualisations of SIRT and CS-ET reconstructions from the tilt-series. The insets (bi) and (ci) are 2D orthoslices from the 3D reconstructions, taken from the positions indicated by the arrows, showing two closely spaced nanoparticles [5].

The two distinct kinds of specimens that are reported here as illustrative examples of ET are (i) specially-prepared iron oxide nanoparticles with a deliberately introduced concavity (for potential use in drug-delivery [18]), and (ii) aggregates of unsupported selective hydrogenation nanocatalysts [19], consisting of nanoparticles in which there is some overlap and partial imbrication; the stoichiometric composition being  $\text{GaPd}_2$ . We also show tomograms that have been obtained, via CS-ET, of cadmium selenide/telluride ‘tetrapods’ [20] associated with concave particles of iron oxide. Preparative methods for these materials and further details of the ET acquisition and post-processing have been given elsewhere [5,18,20–23]. We note however, that all the HAADF-STEM tomography reported here was performed on a standard FEI Tecnai F20 (S)TEM, and the subsequent processing performed using sophisticated yet readily accessible software. Indeed, we emphasise, recalling Fig. 1, ET is a widely accessible technique now practiced in many laboratories.

### 3. Results and discussion

#### 3.1. Concave iron oxide and cadmium selenide/telluride tetrapods

Colloidal iron oxide nanoparticles have attracted growing interest in recent years for their unique performance as catalysts, drug

delivery carriers, mediators in hyperthermia treatments and contrast agents for MRI [18,24,25]. For all of these applications, the structure of the nanoparticles has been demonstrated to be crucial to determining the functional effect. For example, concave iron oxide nanoparticles have been shown to destabilize gold nanocrystals, provided that the size of the gold nanocrystal matches that of the concavity [18].

These nanoparticles were recently used as a model system on which to demonstrate CS-ET. An example HAADF-STEM image of a group of concave iron oxide nanoparticles from an ET tilt-series is shown in Fig. 6a. The tilt-series was recorded over the angular range  $-70^\circ$  to  $+60^\circ$  with a  $5^\circ$  tilt increment. Using the full 27 projection tilt-series, a reconstruction obtained using the conventional algorithm, known as the ‘simultaneous iterative reconstruction technique’ (SIRT), can recover the overall morphology of the nanoparticles to a reasonable, qualitative, approximation. This is shown in the 3D voxel projection visualisation of the reconstruction in Fig. 6b (which provides a projected image analogous to that in the (S)TEM, but with a sense of 3D perspective and visual enhancement by the use of colour). However, quantitative analysis of the structure is challenging owing to artefacts arising from the finite and limited angular sampling. For example, Fig. 6bi shows a 2D slice from the 3D reconstruction, of two nearby nanoparticles. Striking artefacts and blurring in the ‘missing wedge’ direction

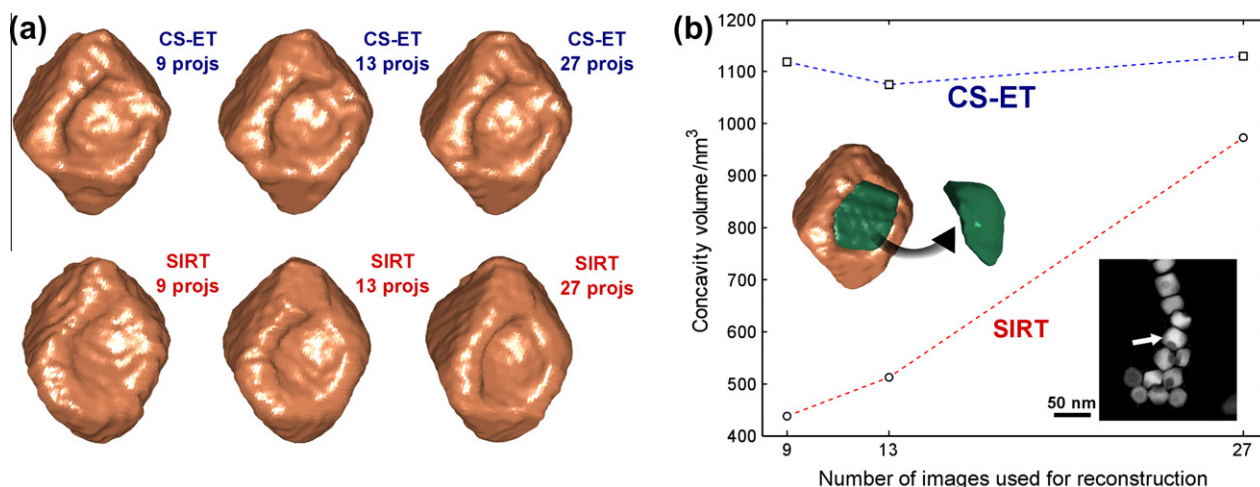


**Fig. 7.** (a) Surface rendered visualisation of CS-ET and SIRT reconstructions from the ET tilt-series of Fig. 6a, using the full 27 projection tilt-series, or 13 or 9 projection subsets. (b) Quantification of the concavity volume of the reconstructions. The nanoparticle analysed is indicated by the arrow in the inset HAADF-STEM image in (b) [5].

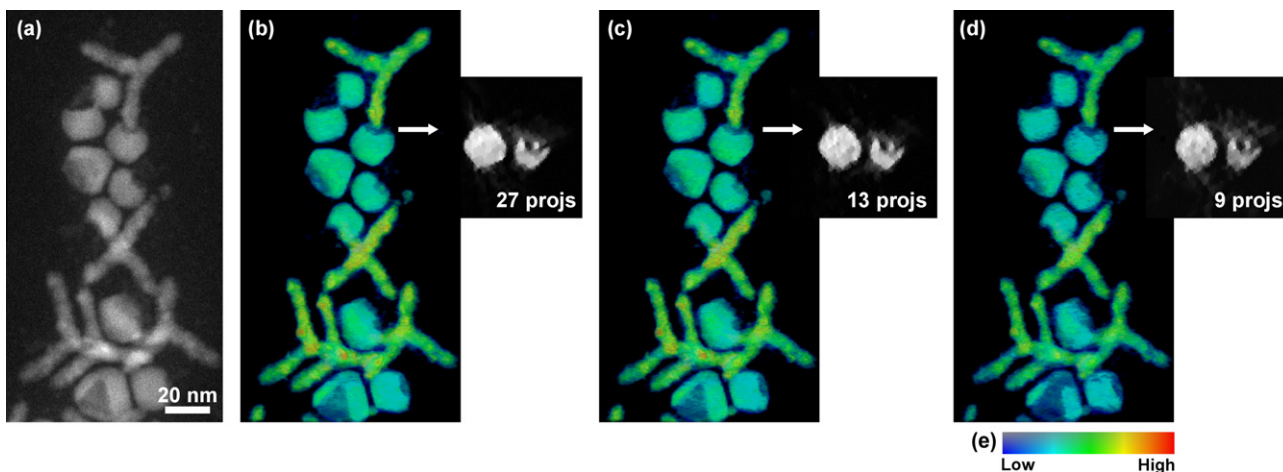


**Fig. 8.** (a) HAADF-STEM image of concave iron oxide nanoparticles interacting with cadmium selenide/telluride tetrapods from an ET tilt-series. (b–d) 3D voxel projection visualisations of CS-ET reconstructions from (b) the full 27 projection tilt-series, as well as (c) 13 projection and (d) 9 projection subsets. (e) Colour map of the 3D voxel projections, revealing atomic number ( $Z$ ) contrast between the nanoparticles and tetrapods. The inset image accompanying each voxel projection is a 2D orthoslice from the 3D reconstruction, taken from the position indicated by the arrow, showing that the reconstruction fidelity in a complex area of the tomogram is largely maintained in the reduced projection reconstructions [23].

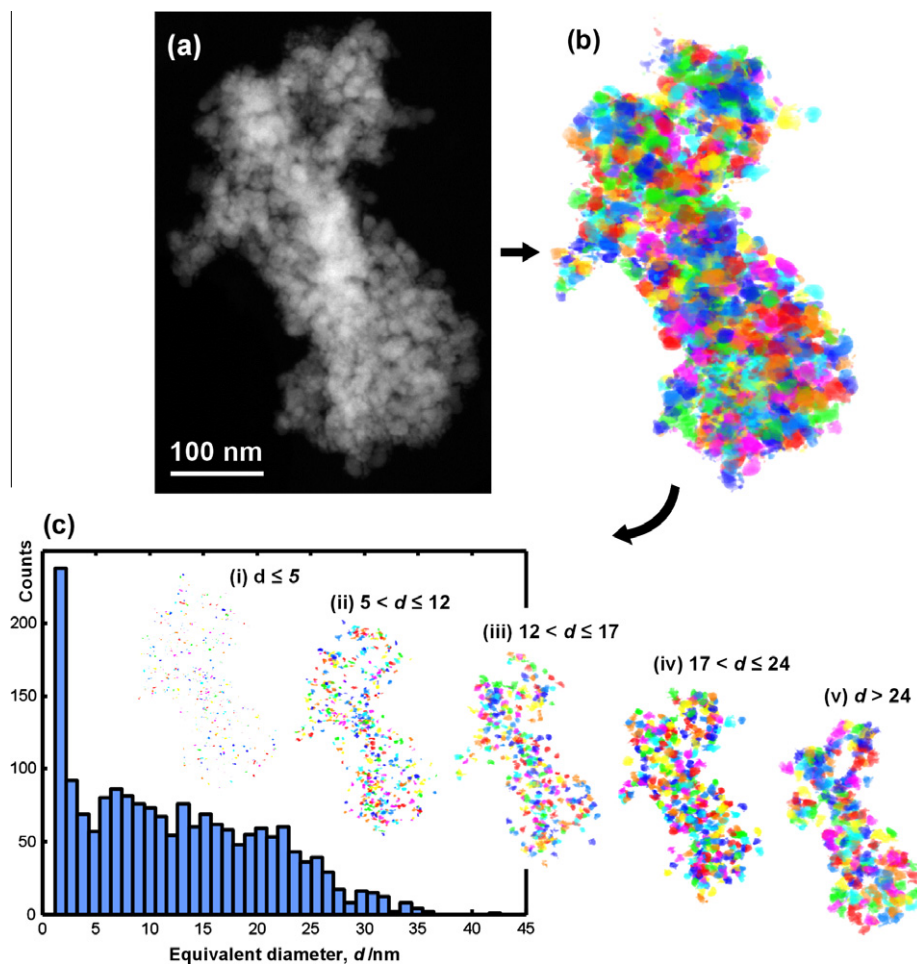


**Fig. 9.** (a) HAADF-STEM image of densely-packed  $\text{GaPd}_2$  nanoparticles from an ET tilt-series. (b) Colour-coded 3D voxel-projection visualisation of the ET reconstruction after segmentation, in which each nanoparticle or agglomerate has been given a colour that differs from those of its nearest neighbours. (c) Statistical size distribution and filtered tomograms according to the equivalent diameter,  $d$ , of the nanoparticles and agglomerates [21].

(the vertical direction in Fig. 6bi and ci) make it difficult to determine the boundary between the two nanoparticles. On the other hand, since the nanoparticles are of uniform composition and should have sharp boundaries, they can be represented sparsely in the gradient domain, and the ET reconstruction can be performed via a CS approach. Using CS-ET yields a high-fidelity reconstruction in which the morphology of the nanoparticles is well-defined, as shown in Fig. 6ci.

The real efficacy of CS is illustrated by performing reconstructions from even fewer projections. Fig. 7a shows 3D reconstructions of a selected nanoparticle (indicated by the arrow in the inset image in Fig. 7b), obtained via both SIRT and CS-ET, and using the full 27 projection tilt-series or just 13 or 9 projection subsets. The volume of the concavity measured from the SIRT reconstructions (Fig. 7b) is seen to decrease as the number of projections is reduced, correlating with the clear loss of reconstruction fidelity seen in Fig. 7a. By contrast, the reconstructed morphology and concavity volume measured from the CS-ET reconstructions is remarkably consistent, even when just 9 projections are used for reconstruction.

In more recent work, we have used CS-ET to provide equally high quality reconstructions of more complex samples, including iron oxide nanoparticles interacting with cadmium selenide/telluride tetrapods (Fig. 8). The different chemical compositions of the nanoparticles and tetrapods leads to atomic number contrast in the HAADF signal, which should be reflected in a different reconstructed intensity (image grey level) for each species. This information is often lost using conventional reconstruction algorithms, but, as shown in Fig. 8, is successfully recovered via CS-ET, even when using just 9 projections. Importantly, CS does not require prior-knowledge of the number of grey levels in the reconstruction, making it applicable to a variety of specimens of unknown composition.

### 3.2. Gallium–palladium selective hydrogenation catalysts

A fundamental difficulty in conventional electron microscopy (TEM or STEM) is the analysis of agglomerates, mixtures and composite structures containing densely-packed nanoparticles, because image interpretation is hampered by multiple particles overlapping when viewed in projection. We illustrate the value of ET in such scenarios by describing our recent analysis [21] of densely-packed nanocrystalline GaPd<sub>2</sub> selective hydrogenation catalysts [19], consisting of nanoparticles and aggregates ca. 1–30 nm in diameter.

Fig. 9a shows an example HAADF-STEM image of the nanoparticles from an ET tilt-series. Semi-automated segmentation (defined below) procedures were applied to the obtained 3D reconstruction, to identify the individual nanoparticles and agglomerates of nanoparticles, which were then colour-coded. (Segmentation of the reconstruction entails assigning each voxel to a feature of interest, e.g. to a nanoparticle, the support or the background. Until recently, segmentation in ET was carried out manually, which is both laborious and prone to user error or bias). The resulting 3D data set (Fig. 9b), in which each nanoparticle or agglomerate of nanoparticles has been assigned a colour that differs from its nearest neighbours, revealed with far greater clarity their 3D morphology and spatial distribution. Moreover, the segmented tomogram could be analysed quantitatively. As an example, Fig. 9c shows in histogram form the size distribution, as well as pictorially the spatial location of nanoparticles and agglomerates in different size ranges.

More recently [26] we have also applied CS-ET to the analysis of these nanocatalysts, obtaining a higher fidelity and more readily segmented reconstruction than when using the conventional SIRT algorithm. We expect CS-ET to play a primary role in the develop-

ment of more robust and routine quantitative nano-metrological studies of these and many other densely-populated nanocluster and nanoparticle systems, including those of particular interest to colloid and interface scientists.

## Acknowledgments

We thank Zineb Saghi and Andrew Sederman for their invaluable role in the development of CS-ET. We are grateful to Chandramohan George, Liberato Manna, Giovanni Bertoni and Andrea Falqui for providing the concave iron oxide nanoparticle and cadmium selenide/telluride tetrapod samples. P.A.M. acknowledges financial support from the ERC, Reference 291522 3DIMAGE.

## Appendix A.1. Compressed sensing and its application to electron tomography

Rowan Leary and Daniel J. Holland.

### A1.1. Introduction

Compressed sensing (CS) [27,28] is a theory that defines the number of measurements required to faithfully reconstruct a signal. Further, it provides guidance as to how these measurements should be obtained. In the following, we outline the key concepts behind CS and its application in electron tomography (ET).

### A1.2. Sparsity

The process of sparse approximation underlies common image compression algorithms such as the JPEG and JPEG-2000 standards, which employ the discrete cosine transform (DCT) and discrete wavelet transform (DWT), respectively, as sparsifying transforms [29]. In these compression schemes, an image is fully sampled and the transform coefficients calculated. The large transform domain coefficients are stored, while the small coefficients are discarded. There may be many more small coefficients than large coefficients, and thus when the small coefficients are discarded, the amount of information representing the image is reduced or ‘compressed.’ An inverse transform of the compressed representation can recover the image with minimal loss of information.

Formally, we begin with a signal  $\mathbf{x}$  (written as a column vector with  $n$  entries or values). This signal could be a spectrum, an image, or in the case of ET, a tomogram. We desire to compress  $\mathbf{x}$ , that is, describe  $\mathbf{x}$  using only a small number of coefficients. To do this, we can express  $\mathbf{x}$  using a linear combination of basis functions  $\psi_i$  (e.g. sinusoids in the case of the DCT):

$$c_i = \sum_{j=1}^n \psi_{ij} x_j \quad (1)$$

where the set of basis functions  $\psi_i$  is chosen such that only  $s$  coefficients of  $\mathbf{c}$  are non-zero. Eq. (1) can be expressed equivalently in matrix form as:

$$\mathbf{c} = \Psi \mathbf{x} \quad (2)$$

where each  $\psi_{ij}$  are the elements of the matrix  $\Psi$ .

If  $s \ll n$ , then  $\mathbf{x}$  is said to be sparsely represented in the basis  $\Psi$ . Another way of describing this is to say that all of the information in  $\mathbf{x}$  is contained in only  $s$  coefficients in the basis  $\Psi$ . If  $\mathbf{x}$  can be well approximated by  $s \ll n$  non-zero coefficients, meaning that there may be many small, negligible coefficients in  $\mathbf{c}$ , which can be set to zero, and only  $s$  significant coefficients,  $\mathbf{x}$  is said to be compressible in  $\Psi$ . A compressible representation in the basis  $\Psi$  captures only the most important information about  $\mathbf{x}$  in  $s$  coefficients.

CS theory uses these ideas of transform sparsity and compressibility during the *initial* acquisition, aiming to acquire a small number of samples that capture just enough information about the signal to be reconstructed. In essence, CS seeks to acquire the signal directly in compressed form.

### A1.3. Sensing

In the CS framework the values of the signal of interest  $\mathbf{x}$  are not observed directly, but rather measurements are made against some test function or sensing waveform  $\phi_i$ . Such a sensing methodology is already common in many practical acquisition schemes. In a conventional imaging process, for example, the sensing waveforms are determined by how the lens maps the scene onto each detector pixel, and the measurements are the intensities at each pixel. In tomography, the sensing waveforms are the projected lines through the sample and the measurements are the line integrals; in magnetic resonance imaging (MRI), the sensing waveforms are sinusoids and the measured data are Fourier coefficients. These measurements are non-adaptive, in that they do not depend on the information content of the signal. Formally,  $m$  correlations are measured between the signal of interest  $\mathbf{x}$  and sensing waveforms  $\phi_i$  from another basis:

$$b_i = \sum_{j=1}^n \phi_{ij} x_j, \quad \text{for } i = 1, \dots, m. \quad (3)$$

which can be abbreviated as:

$$\mathbf{b} = \Phi \mathbf{x} \quad (4)$$

where each  $\phi_i$  represents a row of  $\Phi$ . Incorporating the sparse basis  $\Psi$ , Eq. (4) can be re-written as:

$$\mathbf{b} = \Phi \mathbf{x} = \Phi \Psi^* \mathbf{c} = \Theta \mathbf{c} \quad (5)$$

where  $\Psi^*$  is the inverse transform converting from the sparse basis to the native domain of the signal, and  $\Theta$  is also an  $m \times n$  matrix.

### A1.4. Compressed sensing (CS)

A common occurrence in many practical applications is that there are far fewer measurements than unknowns, that is  $m \ll n$ , and the system of equations is underdetermined, implying there are an infinite number of solutions consistent with the measured data.

CS demonstrates that it is possible to recover  $\mathbf{x}$  in the underdetermined scenario, provided that:

- (1)  $\mathbf{x}$  can be represented sparsely in the basis  $\Psi$ .
- (2)  $\Phi$  and  $\Psi$  are incoherent.

As stated previously, a signal is said to be sparse if it can be represented in a known basis by  $s \ll n$  non-zero coefficients. In the practical application of CS, it is also important to consider signals that are compressible. The condition of compressibility is more general than the strict sparsity condition, enabling CS to be applied to many different signals; in practice, most signals are compressible in some basis, rather than strictly sparse. CS theory states that  $\mathbf{x}$  will be recovered at least as well as the  $s$ -sparse representation or approximation of  $\mathbf{x}$  in the chosen basis. Hence also in the case of compressible signals, this provides a way of tailoring the reconstruction to extract information about the signal at the desired level of complexity, as determined by the level or type of information captured in the compressive representation.

Incoherence essentially entails that the sensing basis is not easily represented in the sparse basis. This ensures that the information from many coefficients of  $\mathbf{x}$  is contained in each

measurement  $b_i$ , and the encoding of the coefficients of  $\mathbf{x}$  is different for each measurement. Another way of interpreting the incoherence condition is that in an incoherent sampling regime, artefacts arising from undersampling add as noise-like interference. This allows the true signal coefficients to be recovered as they stand-out above the interferences. Since it can almost guarantee very high incoherence, randomised sampling has played an important role in the development of CS. (A simple intuitive example of the importance of incoherence is provided in Fig. 2 of [12].)

While in image compression the original image can be recovered simply by applying the inverse transform, CS requires an optimisation process to find the sparse coefficients from the measurements. To achieve this task requires a non-linear algorithm that promotes sparsity, subject to data fidelity. Seeking sparsity by directly minimising the number of non-zeros in the sparse domain is intractable for most real problems. A salient achievement of CS theory has been to show that the minimisation can be performed over the sum of the absolute values, known as the  $\ell_1$ -norm, and defined by  $\|\mathbf{c}\|_{\ell_1} = \sum_i |c_i|$ .

As outlined in [12],  $\ell_1$ -norm minimisation results in a sparse solution because many small coefficients tend to be penalised more than a few larger coefficients; the small coefficients are then suppressed while the important larger coefficients carrying information about the signal in the sparse domain are preserved. In contrast, the more established approach of least squares minimisation, i.e. using the  $\ell_2$ -norm (defined by  $\|\mathbf{c}\|_{\ell_2} = (\sum_i |c_i|^2)^{\frac{1}{2}}$ ) on the regularising term, penalises large coefficients, resulting in smooth solutions with many small coefficients.

The 'standard' CS approach is to solve:

$$\text{minimise } \|\Psi \hat{\mathbf{x}}\|_{\ell_1} \quad \text{subject to } \|\Phi \hat{\mathbf{x}} - \mathbf{b}\|_{\ell_2} \leq \varepsilon \quad (6)$$

where  $\hat{\mathbf{x}}$  is the reconstruction of the true signal  $\mathbf{x}$  from the measured data  $\mathbf{b}$ , and  $\varepsilon$  characterises the standard deviation of the noise in the data. In words, the above minimisation yields the sparsest signal in the transform domain that is consistent with the acquired measurements. Efficient methods have been developed to solve a minimisation over the  $\ell_1$ -norm, such as described by Eq. (6), and there are also other powerful approaches to sparse recovery that can be used, including so-called 'greedy' algorithms and non-convex minimisation. We refer the reader to the recent review by Tropp and Wright [30] for an appropriate overview.

### A1.5. The application of compressed sensing to electron tomography

ET reconstruction can be readily considered in terms of the system of linear equations  $\mathbf{b} = \Phi \mathbf{x}$  dealt with in CS. Specifically, it is possible to consider  $\Phi$  as a real space projection operator, corresponding to some discretized version of the Radon transform, and the data vector  $\mathbf{b}$  as the direct projection data [31]. Alternatively, the Fourier slice theorem (see e.g. [32], chapter 3) may be invoked, which permits the Fourier transform of the projection data to be considered as radial samples of the object in the Fourier domain. The sensing matrix  $\Phi$  can then effectively be considered as an undersampled discrete Fourier operator [5]. In either case, a number of theoretical and experimental papers have demonstrated that CS theory is applicable to projection data such as that obtained in ET [5,12,27,31,33]. However, it is important to note that recovery expectations from experimental ET data should be somewhat more modest than in many of the purely theoretical simulations or other empirical contexts, in particular due to the 'missing wedge' of un-sampled information in Fourier space.

Since a variety of different morphologies can be captured using the various electron microscope imaging modes, it is important to consider the most appropriate sparsifying transform(s) to be used in a CS-ET approach. Owing to the widespread need for sparse

image representation, there are now a range of transforms available for this task [34].

Many electron microscope images and ET reconstructions may be sparse in the image domain itself. Correspondingly, imposing sparsity in the image domain has been demonstrated to reduce ‘streaking’ artefacts and blurring of the object boundaries in ET reconstructions, especially in the missing wedge direction [5]. It is also common in CS to impose sparsity via spatial finite differences, characterised by the ‘total variation’ (TV) in the gradient domain, which is ideal for cartoon-like images that consist of homogenous regions with sharp boundaries (Fig. 5), often referred to as ‘piecewise constant’ images. Such a constraint would be suitable for ET reconstructions of many specimens in the physical sciences that consist of one or a few constituent materials, such as many nanoparticle systems [5,31]. More complex objects can be sparsely represented using, for example, a DWT [35]. The suitability of DWTs for sparsely representing ET data has been demonstrated in DWT-based denoising of biological ET reconstructions [36] and closely related single particle microscopy (SPM) projection images [37], as well as in projection image orientation determination in SPM [38]; and more recently in their CS-based application to SPM 3D reconstruction [39].

## References

- [1] P.A. Midgley, M. Weyland, J.M. Thomas, B.F.G. Johnson, *Chem. Commun.* 18 (2001) 907.
- [2] M. Weyland, P.A. Midgley, J.M. Thomas, *J. Phys. Chem. B* 105 (2001) 7882.
- [3] P.A. Midgley, E.P.W. Ward, A.B. Hungria, J.M. Thomas, *Chem. Soc. Rev.* 36 (2007) 1477.
- [4] J.M. Thomas, P.A. Midgley, *ChemCatChem* 2 (2010) 783.
- [5] Z. Saghii, D.J. Holland, R. Leary, A. Falqui, G. Bertoni, A.J. Sederman, L.F. Gladden, P.A. Midgley, *Nano Lett.* 11 (2011) 4666.
- [6] R. Leary, P.A. Midgley, J.M. Thomas, *Acc. Chem. Res.* (2012), <http://dx.doi.org/10.1021/ar3001102>.
- [7] E. Matijević (Ed.), *Fine Particles in Medicine and Pharmacy*, Springer, New York, 2012 [see in particular: E. Matijević, ‘Preparation of Uniform Drug Particles’, pp. 25–56, and D.V. Goia & T.K. Sau, ‘Biomedical Applications of Gold Nanoparticles’, pp. 101–146].
- [8] N. Korin, M. Kanapathipillai, B.D. Matthews, M. Crescente, A. Brill, T. Mammoto, K. Ghosh, S. Jurek, S.A. Bencherif, D. Bhatta, A.U. Coskun, C.L. Feldman, D.D. Wagner, D.E. Ingber, *Science* (2012), <http://dx.doi.org/10.1126/science.1217815>.
- [9] A.J. Koster, U. Ziese, A.J. Verkleij, A.H. Janssen, K.P. de Jong, *J. Phys. Chem. B* 104 (2000) 9368.
- [10] J.M. Thomas, P.A. Midgley, T.J.V. Yates, J.S. Barnard, R. Raja, I. Arslan, M. Weyland, *Angew. Chem., Int. Edit.* 43 (2004) 6745.
- [11] E.P.W. Ward, T.J.V. Yates, J.-J. Fernández, D.E.W. Vaughan, P.A. Midgley, *J. Phys. Chem. C* 111 (2007) 11501.
- [12] M. Lustig, D. Donoho, J.M. Pauly, *Magn. Reson. Med.* 58 (2007) 1182.
- [13] D.J. Holland, D.M. Malioutov, A. Blake, A.J. Sederman, L.F. Gladden, *J. Magn. Reson.* 203 (2010) 236.
- [14] M.F. Duarte, M.A. Davenport, D. Takhar, J.N. Laska, S. Ting, K.F. Kelly, R.G. Baraniuk, *IEEE Signal Proc. Mag.* 25 (2008) 83.
- [15] E.J. Candès, M.B. Wakin, *IEEE Signal Proc. Mag.* 25 (2008) 21.
- [16] R.G. Baraniuk, *IEEE Signal Proc. Mag.* 24 (2007) 118.
- [17] J. Romberg, *IEEE Signal Proc. Mag.* 25 (2008) 14.
- [18] C. George, D. Dorfs, G. Bertoni, A. Falqui, A. Genovese, T. Pellegrino, A. Roig, A. Quarta, R. Comparelli, M.L. Curri, R. Cingolani, L. Manna, *J. Am. Chem. Soc.* 133 (2011) 2205.
- [19] M. Armbrüster, K. Kovnir, M. Behrens, D. Teschner, Y. Grin, R. Schlögl, *J. Am. Chem. Soc.* 132 (2010) 14745.
- [20] A. Fiore, R. Mastroia, M.G. Lupo, G. Lanzani, C. Giannini, E. Carlino, G. Morello, M. De Giorgi, Y. Li, R. Cingolani, L. Manna, *J. Am. Chem. Soc.* 131 (2009) 2274.
- [21] R. Leary, Z. Saghii, M. Armbrüster, G. Wowsnick, R. Schlögl, J.M. Thomas, P.A. Midgley, *J. Phys. Chem. C* 116 (2012) 13343.
- [22] M. Armbrüster, G. Wowsnick, M. Friedrich, M. Heggen, R. Cardoso-Gil, *J. Am. Chem. Soc.* 133 (2011) 9112.
- [23] R. Leary, Z. Saghii, A.J. Sederman, J.M. Thomas, L.F. Gladden, M. Armbrüster, R. Schlögl, P.A. Midgley, D.J. Holland, Presentation at: 2nd International Symposium on Advanced Electron Microscopy for Catalysis and Energy Storage Materials (EmCat-2012), February 5th–8th, 2012, Berlin, Germany.
- [24] A.A. Herzing, C.J. Kiely, A.F. Carley, P. Landon, G.J. Hutchings, *Science* 321 (2008) 1331.
- [25] A. Figuerola, R. Di Corato, L. Manna, T. Pellegrino, *Pharmacol. Res.* 62 (2010) 126.
- [26] R. Leary, et al., in preparation.
- [27] E.J. Candès, J. Romberg, T. Tao, *IEEE Trans. Inf. Theory* 52 (2006) 489.
- [28] D.L. Donoho, *IEEE Trans. Inf. Theory* 52 (2006) 1289.
- [29] D.S. Taubman, M.W. Marcellin, *Proc. IEEE* 90 (2002) 1336.
- [30] J.A. Tropp, S.J. Wright, *Proc. IEEE* 98 (2010) 948.
- [31] B. Goris, W. Van den Broek, K.J. Batenburg, H. Heidari Mezerji, S. Bals, *Ultramicroscopy* 113 (2012) 120.
- [32] A.C. Kak, M. Slaney, *Principles of Computerized Tomographic Imaging*, IEEE Press, New York, 1988.
- [33] E.Y. Sidky, X.C. Pan, *Phys. Med. Biol.* 53 (2008) 4777.
- [34] J.L. Starck, F. Murtagh, J.M. Fadili, *Sparse Image and Signal Processing: Wavelets, Curvelets, Morphological Diversity*, Cambridge University Press, Cambridge, 2010.
- [35] S. Mallat, *A Wavelet Tour of Signal Processing*, Academic Press, Burlington, MA, 2008.
- [36] A. Stoschek, R. Hegerl, *J. Struct. Biol.* 120 (1997) 257.
- [37] C.O.S. Sorzano, E. Ortiz, M. López, J. Rodrigo, *Pattern Recogn.* 39 (2006) 1205.
- [38] C.O.S. Sorzano, S. Jonić, C. El-Bez, J.M. Carazo, S. De Carlo, P. Thévenaz, M. Unser, *J. Struct. Biol.* 146 (2004) 381.
- [39] C. Vonesch, W. Lanhui, Y. Shkolnisky, A. Singer, in: *IEEE International Symposium on Biomedical Imaging: From Nano to Macro*, March 30th–April 2nd, Chicago, Illinois, USA, 2011, p. 1950.